

## Article

# Three-Dimensional Static and Dynamic Analyses of an Embedded Concrete-Face Rockfill Dam

Pengfei Qu, Junrui Chai \*  and Zengguang Xu

State Key Laboratory of Eco-Hydraulics in Northwest Arid Region of China, Xi'an University of Technology, Xi'an 710048, China; unique\_0106@126.com (P.Q.); xuzengguang@xaut.edu.cn (Z.X.)

\* Correspondence: jrchai@xaut.edu.cn

**Abstract:** Concrete-face rockfill dams have gradually become the preferred dam type in the engineering community. This study presents a hydropower station in China as a case study to introduce a new type of embedded concrete-face rockfill dam. The static and dynamic stress–strain characteristics of the proposed and conventional concrete-face rockfill dams were compared, and the optimal height of the embedded concrete body at the hydropower station was determined. The results indicate that, under static conditions, the embedded concrete body could reduce deformation upstream and downstream of the rockfill body, eliminate tensile stress along the concrete-face slab slope, reduce concrete-face slab deflection, and increase the maximum deflection area to 0.47 times the dam height. The inhibitory effect of the embedded concrete body on the stress and strain of the dam body became more evident as the size of the embedded body increased. Although the embedded concrete body did not enhance the dynamic and superposed static–dynamic stress states of the embedded concrete body and rockfill, the stress and strain increase in the dynamic state were within a controllable range. Through a sensitivity analysis and considering the terrain conditions and engineering cost of the hydropower station, the height of the embedded concrete body is recommended to be 0.4 times the dam height.

**Keywords:** embedded concrete-face rockfill dam; concrete-face slab; numerical calculation; deformation characteristics; mechanical properties



**Citation:** Qu, P.; Chai, J.; Xu, Z.

Three-Dimensional Static and Dynamic Analyses of an Embedded Concrete-Face Rockfill Dam. *Water* **2023**, *15*, 4189. <https://doi.org/10.3390/w15234189>

Academic Editors: Pingping Luo, Aidi Huo and Chunli Zheng

Received: 6 November 2023

Revised: 28 November 2023

Accepted: 30 November 2023

Published: 4 December 2023



**Copyright:** © 2023 by the authors. Licensee MDPI, Basel, Switzerland. This article is an open access article distributed under the terms and conditions of the Creative Commons Attribution (CC BY) license (<https://creativecommons.org/licenses/by/4.0/>).

## 1. Introduction

Concrete-face rockfill dams have gradually become the preferred dam type in the engineering community owing to their safety, affordability, and applicability in complex terrain and climatic conditions [1–3]. The construction height of concrete-face rockfill dams has exceeded 240 m and is increasing towards 300 m [4–6]. As the only anti-seepage structure in such dams, the structural safety and integrity of the concrete-face slab are extremely important [7,8]. Consequently, with increasing construction heights and enhanced complex deformation coordination problems related to concrete-face slabs, analyses of the static and dynamic mechanics and deformation characteristics of concrete-face rockfill dams have become common methods for evaluating the stress and strain characteristics of concrete-face slabs and rockfills [9,10].

Kim et al. [11] analysed the stress–strain characteristics of the Daegok concrete-face rockfill dam in South Korea during its construction and found that disturbances caused by the dam filling had little effect on the concrete-face slab. Instead, the concrete-face slab deformation was caused by the water load and uneven settling after the dam was impounded. Their calculated results were also consistent with the monitoring results. Liu et al. [12] used static and dynamic calculations to determine that the potential cracking area of the concrete-face slab during the operational period was concentrated in the middle and lower parts of the slab, which was consistent with the measured results. Based on finite element analysis of the Shuibuya concrete-face rockfill dam in China, Yao et al. [13]

proposed a response surface method and improved genetic algorithm, successfully obtained the calculation parameters of the Duncan E-B and creep models, and predicted the settlement of the dam. Xu et al. [14] focused on the dynamic characteristics of concrete-face rockfill dams under earthquake excitation conditions and found that tensile damage to the concrete-face slab following an earthquake was concentrated in regions located at 0.65 and 0.85 times the dam height. The dynamic calculation method can quickly and accurately determine the location of damage to the concrete-face slab. Kartal et al. [15] used the improved Rackwitz–Fiessler method to analyse the static effect of the Torul concrete-face rockfill dam in Turkey. This method considered the geometric nonlinearity of the dam body and the interactions between the concrete-face slab and rockfill foundation, from which the critical failure location and failure probability of the concrete-face slab were determined. Similarly, Wen et al. [16] analysed the influence of foundation overburden depth on dam body deformation at the Miaojiaba concrete-face rockfill dam in China. Concrete-face slab deflection increased by approximately 0.1% when the dam was built on a gravel foundation, and the calculated results were consistent with the monitoring data. These previous studies indicate that the stress and deformation characteristics of high concrete-face rockfill dams under complex conditions can be determined accurately using static and dynamic calculations, which are crucial for engineering construction and management [17–19].

Previous studies have also indicated that deformation is uncoordinated during the settlement of the dam body owing to the rigidity of the concrete-face slab, which increases the risk of slab cracking and failure and can seriously affect the anti-seepage performance of the dam body. This problem is particularly noticeable in high concrete-face rockfill dams. To address this problem, the China Electric Power Construction Group Northwest Survey and Design Institute Co., Ltd. proposed the construction of a new embedded concrete-face rockfill dam (ECFRD) at a hydropower station in China (Figure 1) based on a conventional concrete-face rockfill dam (CCFRD). In the ECFRD, the embedded concrete body was placed at the heel of the dam and connected to the concrete-face slab to form a complete impervious body, thereby shortening the lengths of the concrete-face slab and joint and bearing part of the force on the concrete-face slab to limit deformation of the dam body. This new ECFRD aimed to improve the acceptance conditions of the high concrete-face rockfill dam and improve its adaptability.

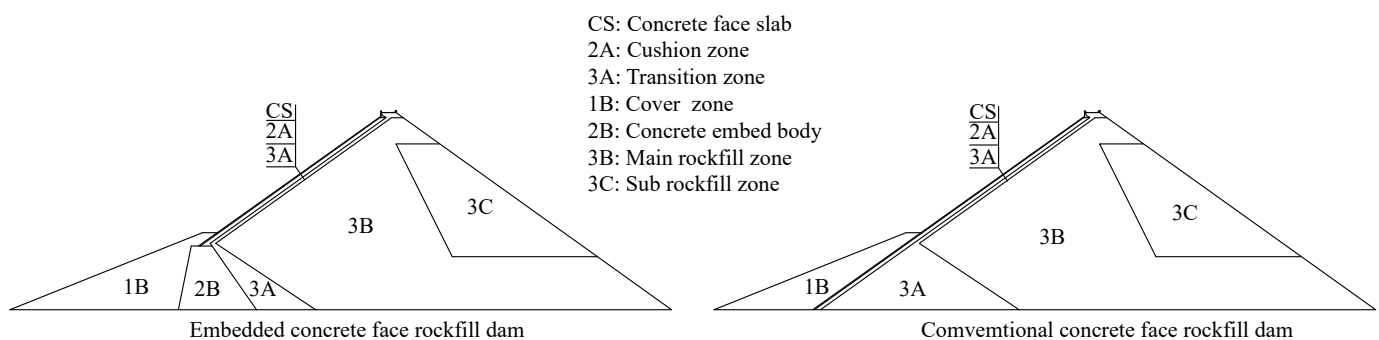


**Figure 1.** Cross-sections of embedded and conventional concrete-face rockfill dams.

In this study, the abovementioned hydropower station in China was used as a case study. Finite element analysis was performed based on static and dynamic analysis methods. The stress and strain characteristics of the rockfill and concrete-face slabs of the ECFRD and CCFRD scenarios were compared and analysed, and the influence of the embedded concrete body on the stress distribution and deformation characteristics of the dam body was determined. The optimal height of the embedded concrete body was then determined using sensitivity analysis, and the dynamic stress–strain characteristics of the ECFRD under seismic excitation conditions were analysed. The findings of this study can be used to provide a new design concept for the construction of 200~300 m concrete-face rockfill dams.

## 2. Computational Methods

### 2.1. Project Profile

The hydropower station addressed in this study is located in Qinghai Province, China. The station is dominated by power generation, with a storage capacity of 14.724 billion m<sup>3</sup> and a total installed power generation capacity of 1200 MW. An ECFRD was adopted for the first time in a water-retaining structure at the station, with a maximum dam height of 150 m. A cross-section of the dam is shown in Figure 2, and the layout of the dam site is shown in Figure 3. The dam body can be divided into a concrete-face slab, cover zone, cushion zone, embedded concrete body, transition zone, main rockfill zone, sub-rockfill zone, and embedded concrete body and dam heel positions. The earthquake intensity in the engineering area was set to VII on the modified Mercalli intensity scale, with a peak acceleration of 0.304 g and a 100-year exceedance probability of 2%. The seismic time-history curve of the hydropower station is shown in Figure 4.

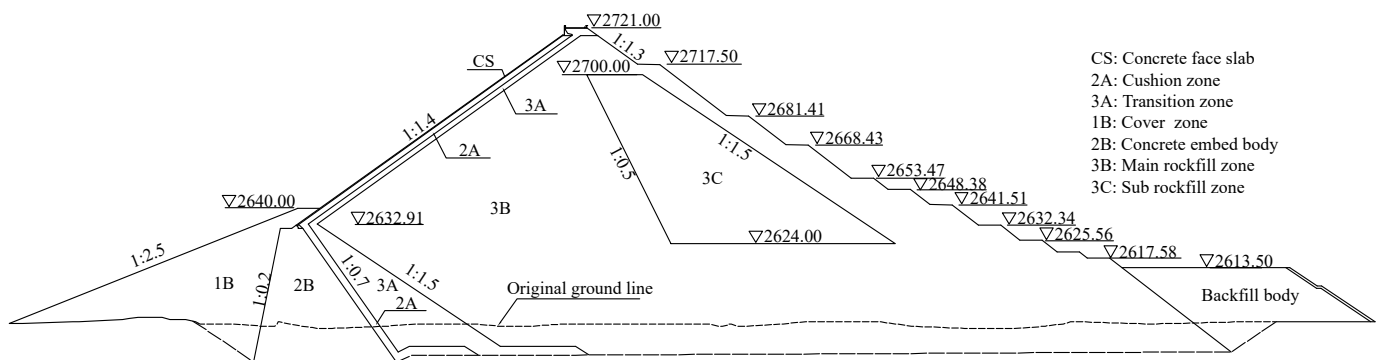


**Figure 2.** Cross-sectional drawing of the embedded concrete-face rockfill dam (ECFRD) hydropower station.

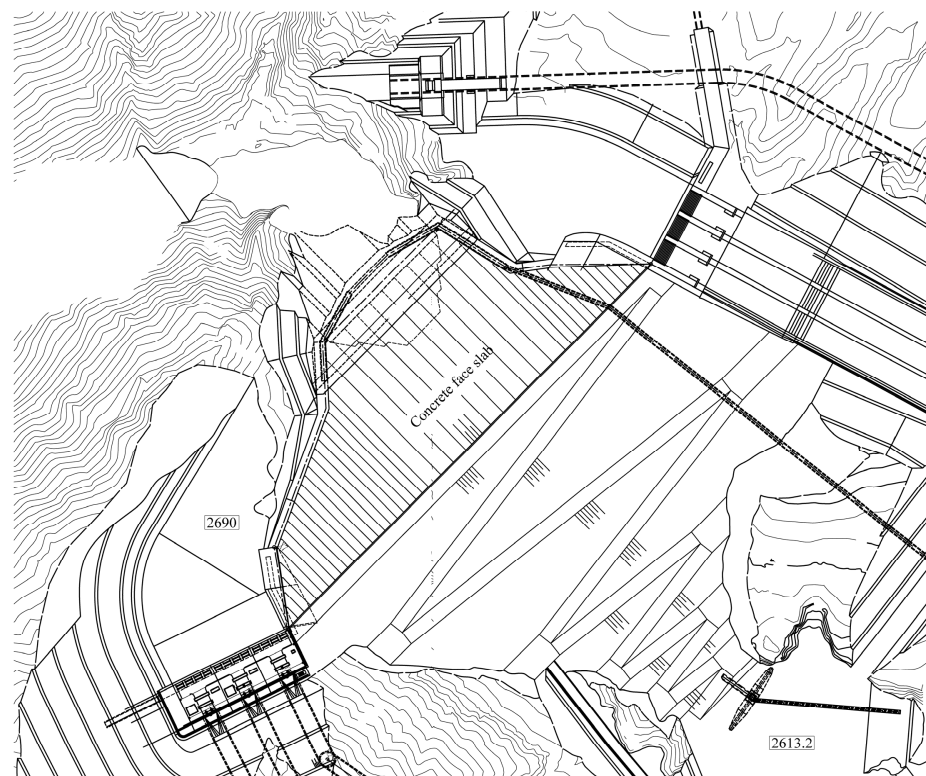


**Figure 3.** Layout of the dam at the hydropower station assessed in this study.

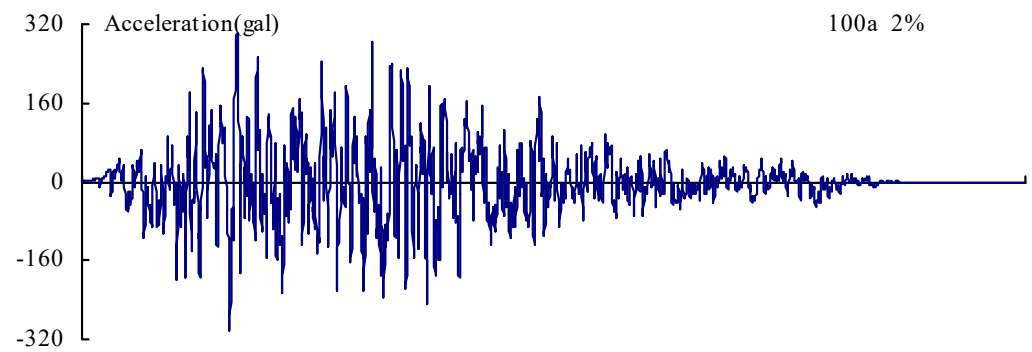


**Figure 4.** Seismic time-history curve for the hydropower station, with a 100-year exceedance probability of 2%.

## 2.2. Finite Element Modelling and Parameters

**Simulation model:** The three-dimensional finite element mesh generated for the ECFRD at the hydropower station is shown in Figure 5. The 8-node hexahedral isoparametric spatial element was adopted in this study. To adapt to changes in the dam boundary conditions, the boundary part was degenerated into a triangular prism or tetrahedral element, which was divided into 16,913 elements and 19,402 nodes.

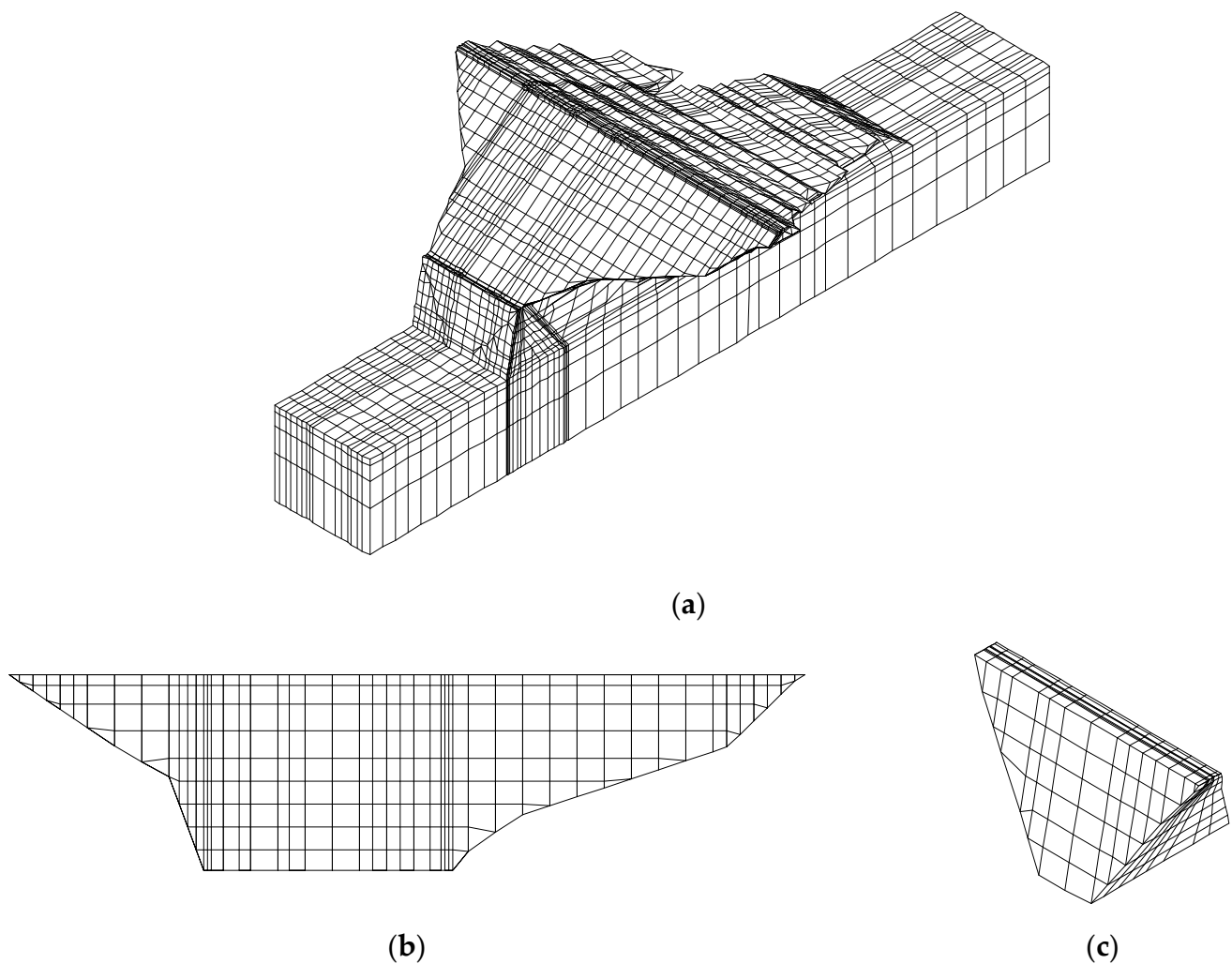


**Figure 5.** Static and dynamic calculation models used for the ECFRD. (a) Unitary model; (b) Concrete-face slab model; (c) Embedded concrete body model.

**Boundary conditions:** The bedrock depth at the hydropower station was approximately 90 m. The lower boundary of the model had an elevation of 2481 m, which was fixed. The upstream and downstream truncation boundaries were set to 150 m from the foot of the dam and acted as lateral constraints. The main loading on the dam included the water load, weight of the dam body, and seismic dynamics.

**Material behaviour:** The experimentally obtained Duncan–Chang E-B model parameters of the main dam materials are listed in Table 1, and the elastic parameters of the concrete materials and ground baseline are listed in Table 2.

**Table 1.** Duncan–Chang E-B model parameters of the main dam materials.

Dam Material	Density (g/cm <sup>3</sup> )	Angle of Internal Friction (°)	Elastic Modulus	Initial Stiffness Index	Damage Ratio	Volume Compression Modulus Coefficient	Volume Deformation Modulus Coefficient	Unloading-Repeated Addition Coefficient
2A	2.25	54.8	1023.3	0.32	0.61	500.0	0.25	2046.6
3A	2.17	56.2	1438.6	0.23	0.72	791.5	0.02	2877.2
3B	2.15	56.6	1412.5	0.22	0.72	772.2	0.04	2825.0
3C	2.15	52.2	800.0	0.26	0.62	400.0	0.29	1600.0

**Table 2.** Calculated elastic parameters of the concrete materials and ground baseline.

Material	Density (g/cm <sup>3</sup> )	Elastic Modulus (GPa)	Poisson Ratio
CS	2.4	28	0.167
2B	2.4	30	0.167
Foundation	2.7	11.9	0.167

**Convergence criteria:** Forced convergence was preferred in this study, with a default criterion value of 0.5% and a minimum residual reference value of 0.01 N.

### 3. Influence of the Embedded Concrete Body on the Static Characteristics of the Dam

To demonstrate the role and advantages of the embedded concrete body, we compared and analysed the stress and strain characteristics of the dam body using an ECFRD and CCFRD. The height of the embedded concrete body was 40 m, which was the only difference between the two dam types.

#### 3.1. Rockfill Body Strain Analysis

Because the rockfill is granular and undergoes compressive stress, we focused only on its strain characteristics. The calculated strains for the two dam types under normal water levels are shown in Figure 6 and Table 3. For the CCFRD, the maximum horizontal displacements upstream and downstream of the rockfill body were 5.0 and 7.4 cm, respectively. The maximum settlement of the rockfill body was 46.2 cm, located near half the dam height, which accounted for 0.3% of the dam height. For the ECFRD, the maximum horizontal displacements upstream and downstream of the rockfill body were 2.9 and 6.8 cm, respectively, and the maximum settlement of the rockfill body was 45.6 cm. These results indicate that the embedded concrete body effectively reduced the upstream and downstream deformation of the concrete-face rockfill dam and slightly reduced the settlement of the rockfill body.

**Table 3.** Deformation results for the dam rockfill in the CCFRD and ECFRD.

Dam Type	Settlement (cm)	Upstream Deformation (cm)	Downstream Deformation (cm)
CCFRD	46.2	5.0	7.4
ECFRD	45.6	2.9	6.8

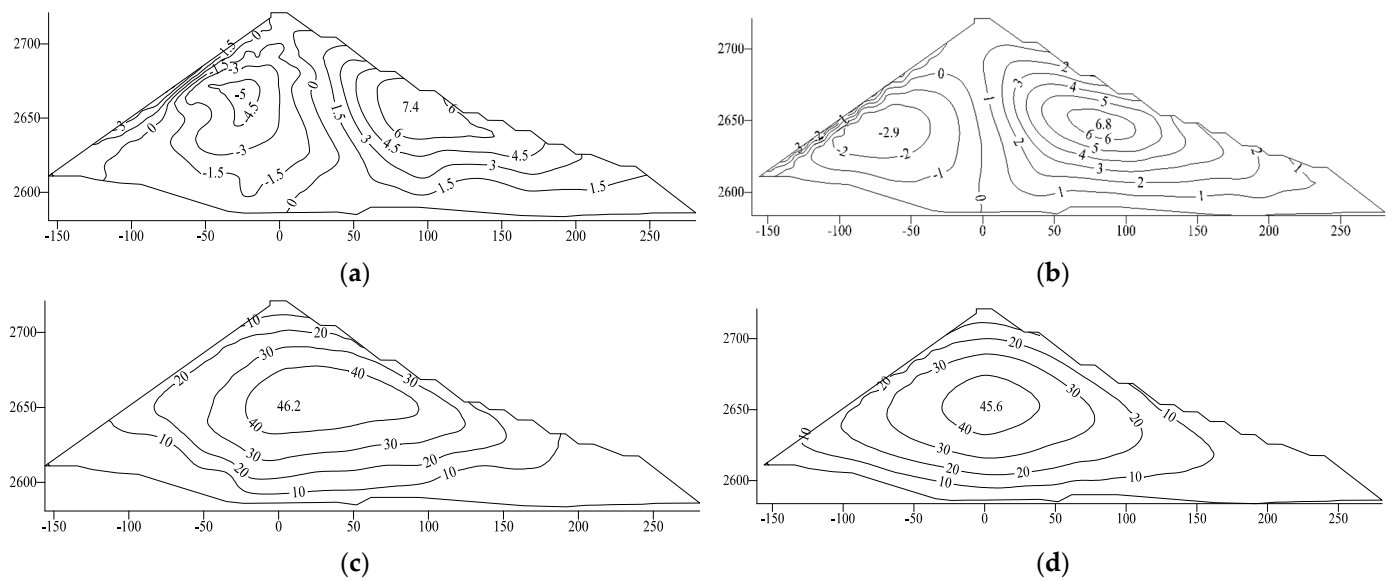


**Figure 6.** Calculated strain for the maximum rockfill cross-section in the dam body (cm). (a) CCFRD rockfill displacement along the river; (b) ECFRD rockfill displacement along the river; (c) CCFRD rockfill settlement; (d) ECFRD rockfill settlement.

### 3.2. Concrete-Face Slab Stress–Strain Analysis

The stress and strain results for the two dam types under normal water-level conditions are shown in Figures 7 and 8, and Table 4. Figure 7 and Table 4 show that the concrete-face slab was primarily compressed and partially pulled when a CCFRD was used in the dam. During the impoundment period, the maximum axial compressive and tensile stresses on the concrete-face slab were 6.43 and 1.15 MPa, respectively, while the maximum compressive and tensile stresses along the slope were 8.27 and 0.16 MPa, respectively. When an ECFRD was used in the dam, the concrete-face slab was only partially tensioned in the axial direction on both sides, with maximum axial compressive and tensile stresses of 5.64 and 0.86 MPa, respectively. Thus, the tensile stress on the concrete-face slab along the slope decreased, with a maximum compressive stress of 6.95 MPa.

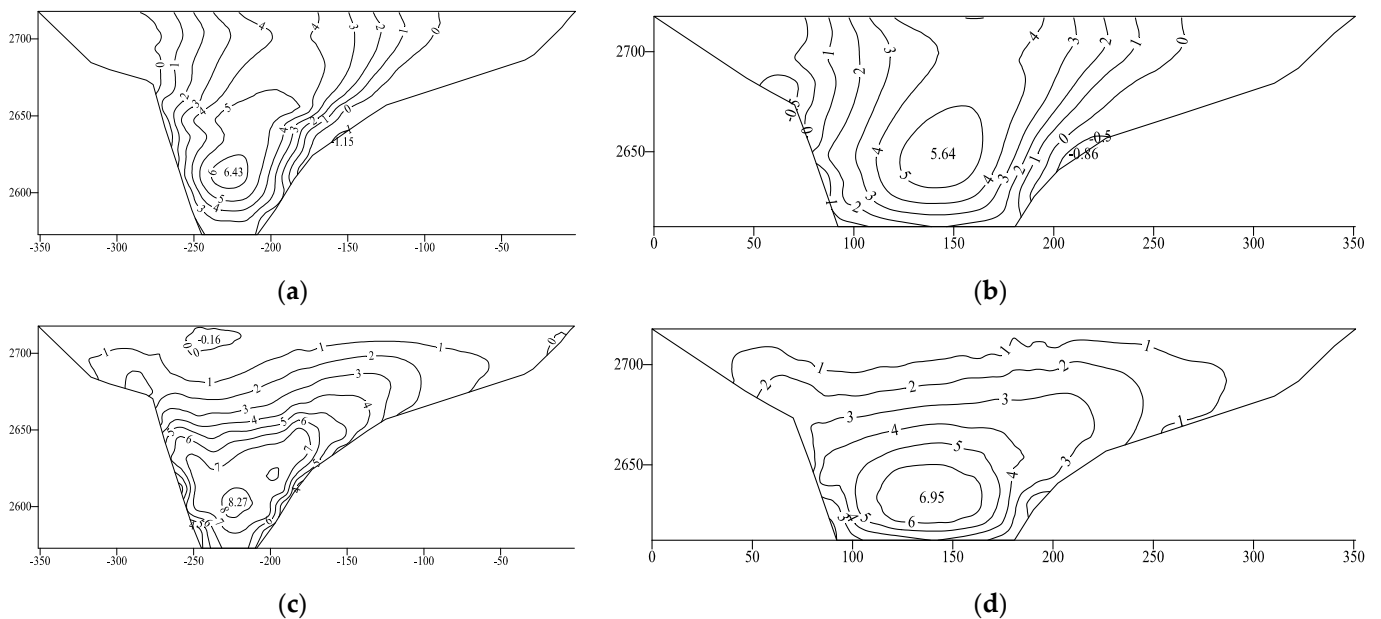


**Figure 7.** Stresses on the concrete-face slab in the CCFRD and ECFRD. Negative values indicate tensile stress (MPa). (a) Axial stress on the CCFRD concrete-face slab; (b) Axial stress on the ECFRD concrete-face slab; (c) Slope stress on the CCFRD concrete-face slab; (d) Slope stress on the ECFRD concrete-face slab.

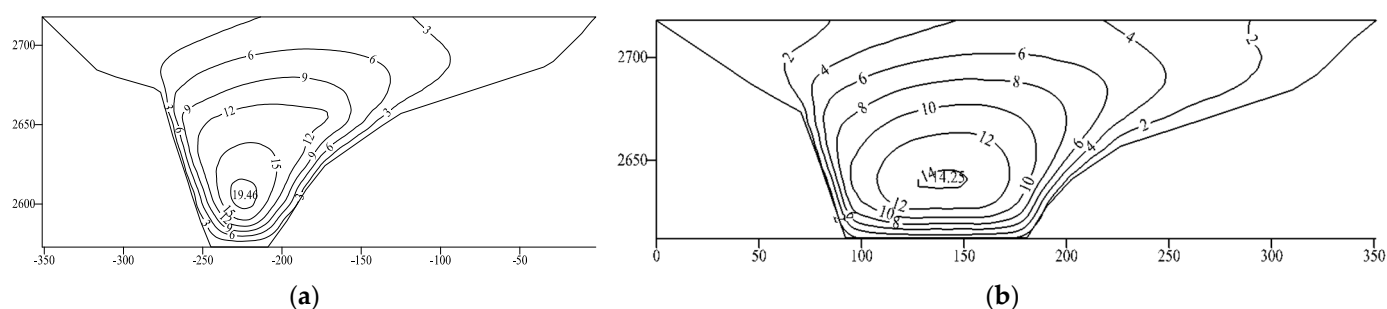


**Figure 8.** Concrete-face slab deflection in the CCFRD and ECFRD (cm). (a) Deflection of the CCFRD concrete-face slab; (b) Deflection of the ECFRD concrete-face slab.

**Table 4.** Concrete-face slab deformation and strain results for the CCFRD and ECFRD.

Dam Type	Axial Compressive Stress (MPa)	Axial Tensile Stress (MPa)	Compressive Stress along the Slope (MPa)	Tensile Stress along the Slope (MPa)	Deflection (cm)
CCFRD	6.34	1.15	8.27	0.16	19.46
ECFRD	5.64	0.86	6.95	/	6.8

In addition, Figure 8 and Table 4 indicate that the maximum deflection of the concrete-face slab was 19.46 cm at an elevation of 2602 m on the left side of the dam when a CCFRD was used. Since the lower part of the valley that contains the dam is extremely steep, the location of the concrete-face slab deflection was low, approximately 0.21 times the dam height. When an ECFRD was used, the area and length of the concrete-face slab decreased, and the maximum deflection decreased to 14.25 cm. The location of the maximum deflection also changed to an elevation of 2642 m on the left side of the dam, which was approximately 0.47 times the dam height.

The results indicate that, in the construction of a 150 m tall concrete-face rockfill dam, an embedded concrete body could effectively reduce the stress on the concrete-face slab, reduce concrete-face slab deflection, and compress the concrete-face slab along the slope, thereby reducing the possibility of tensile failure.

### 3.3. Sensitivity Analysis of the Embedded Concrete Body Height

To analyse the influence of the embedded concrete body height on the stress and strain characteristics of the rockfill and concrete-face slab and to determine the optimal height of the embedded concrete body at the hydropower station, we adjusted the height of the embedded concrete body to 50, 60, and 70 m (based on the model shown in Figure 5). The stress and strain maxima for the rockfill, concrete-face slab, and embedded concrete body during the impoundment period are shown in Figures 9–11, respectively. The results indicate that the settlement of the rockfill and the upstream and downstream deformation decreased as the height of the embedded concrete body increased. The height of the embedded concrete body exceeded 0.3 times the dam height, which had a considerable influence on controlling the rockfill deformation. Similarly, the length of the concrete-face slab and the deflection, axial, and slope stresses on the concrete-face slab all decreased as the height of the embedded concrete body increased. Overall, a taller embedded concrete body could improve the stress–strain characteristics of the rockfill and concrete-face slab, thereby improving the stability of the dam body and the integrity of the concrete-face slab structure.

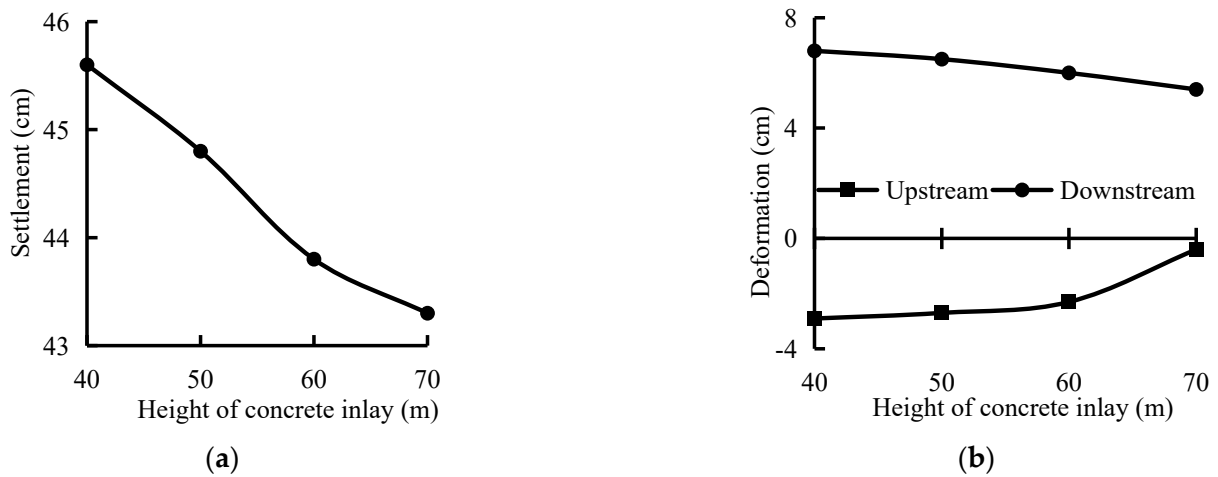


**Figure 9.** Influence of the height of the embedded concrete body on the stress–strain characteristics of the rockfill. (a) Variations in rockfill settlement; (b) Upstream and downstream deformation of rockfill.

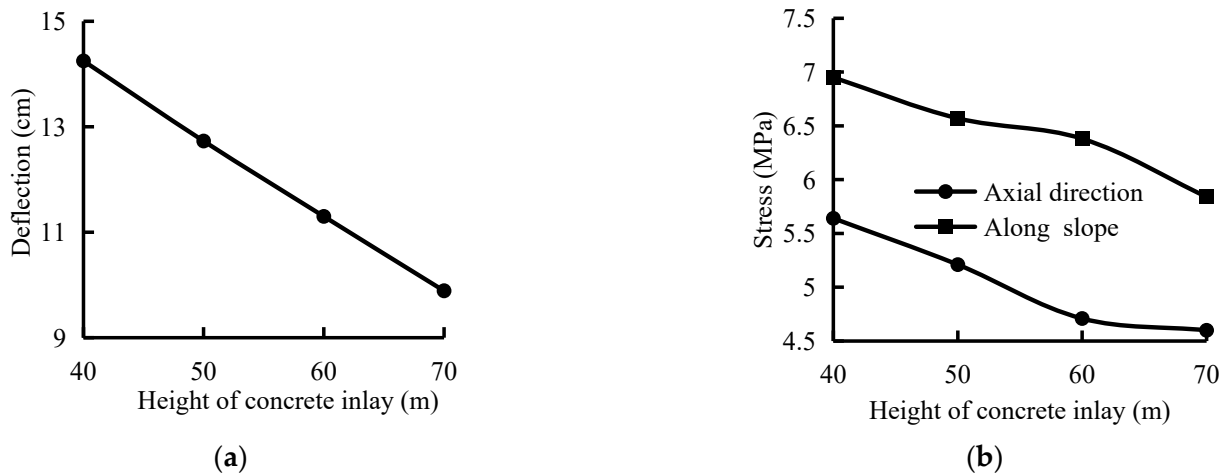


**Figure 10.** Influence of the height of the embedded concrete body on the stress–strain characteristics of the concrete-face slab. (a) Deflection of the concrete-face slab; (b) Stress deformation of the concrete-face slab.

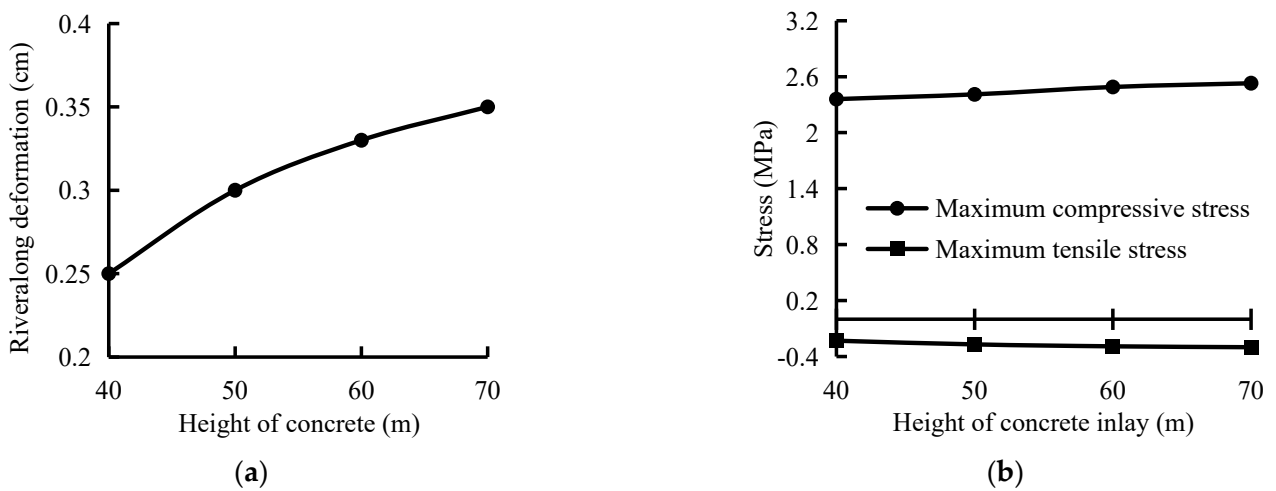


**Figure 11.** Influence of the height of the embedded concrete body on its stress–strain characteristics. (a) Deformation of the embedded concrete body along the river; (b) Stress changes in the embedded concrete body.

However, as shown in Figure 11, the tensile stress, compressive stress, and deformation along the river increased as the height of the embedded concrete body increased. Although the deformation range and stress value of the embedded concrete body were within the allowable range of the concrete material, the width of the main tensile stress zone was less than 0.07 times the width of the bottom surface. However, when the height of the embedded concrete body was greater than 60 m, the river valley at the dam site area was open, the construction volume of the embedded concrete body and its contact area with the cushion layer increased, and construction difficulties were minor. The improved stress conditions and the degeneration limit of the concrete-face slab and rockfill also met engineering requirements. Consequently, we recommend that the height of the embedded concrete body in a dam with dimensions similar to those of the dam at the hydropower station should be 60 m, which is 0.4 times the dam height.

**4. Dynamic Deformation Analyses**

*4.1. Rockfill Dynamic Deformation Analysis*

For the CCFRD and ECFRD schemes with an embedded concrete body height of 60 m, when the bedrock exceeded the probability of 2% earthquake peak acceleration (0.304 g) in 100 years, the deformation of the rockfill was caused by static and dynamic superposition that resulted in permanent deformation (Figure 12 and Table 5). The results indicate that the maximum dynamic displacement of the CCFRD rockfill in the river and vertical directions were 13.1 and 6.3 cm, respectively. Permanent deformation in the river direction manifested as downstream deformation (maximum of 19.9 cm). Permanent deformation in the vertical direction manifested as seismic subsidence (maximum of 27.7 cm). For the ECFRD, the maximum dynamic displacements of the rockfill in the river and vertical directions were 17.1 and 7.5 cm, respectively, with corresponding permanent deformations of 21.6 and 31.3 cm, respectively.

**Table 5.** Rockfill deformation in the CCFRD and ECFRD (cm) under earthquake action.

Dam Type	Displacement along the River	Vertical Deformation	Permanent Deformation along the River	Permanent Vertical Deformation
CCFRD	13.1	6.3	19.9	27.7
ECFRD	17.1	7.5	21.6	31.3

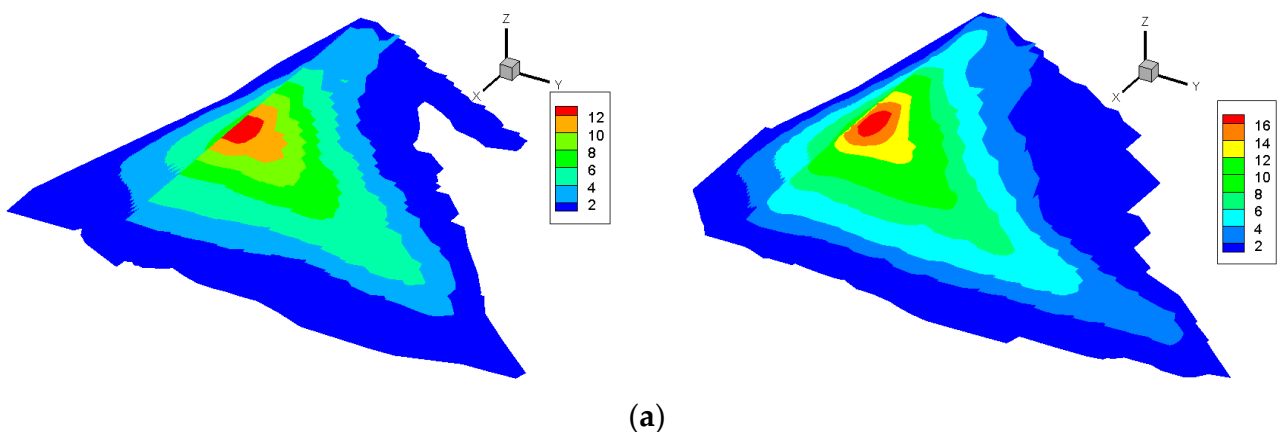


**Figure 12.** *Cont.*

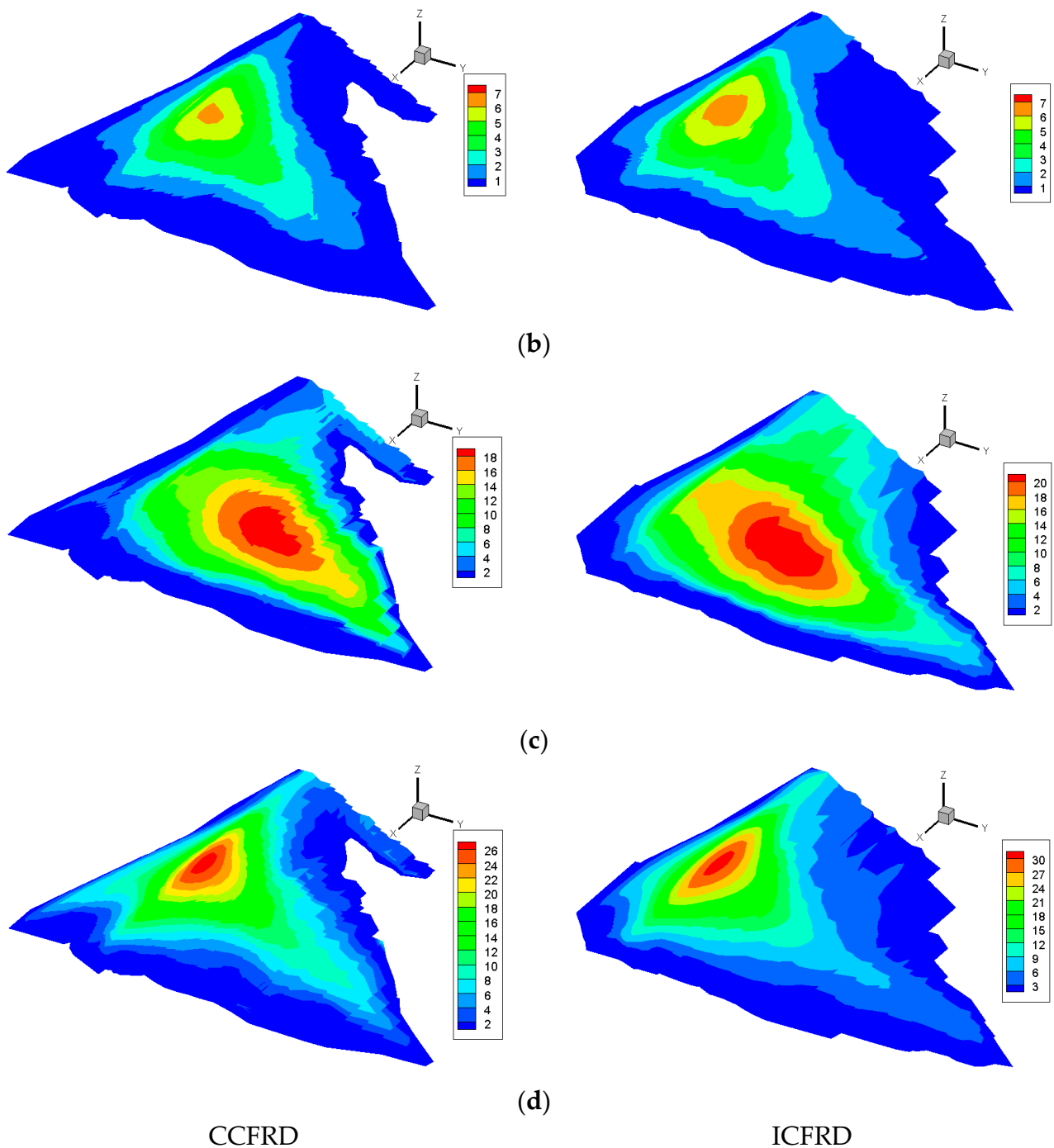


**Figure 12.** Calculated rockfill deformation in the CCFRD and ECFRD under earthquake action (cm). (a) Displacement along the river under earthquake action; (b) Vertical deformation under earthquake action; (c) Permanent deformation along the river under earthquake action; (d) Permanent vertical deformation under earthquake action.

#### 4.2. Dynamic and Static–Dynamic Deformation Analyses of the Concrete-Face Slab

The results of the dynamic and static–dynamic superposition of the concrete-face slab under earthquake conditions are shown in Figures 13 and 14, respectively, and Table 6. The results indicate that the tensile stress on the concrete-face slab was the main cause of its cracking. Consequently, we focused only on the distribution law and superposition state of the dynamic tensile stress under earthquake conditions. Figure 13 and Table 6 indicate that the maximum deflection of the concrete-face slab in the CCFRD caused by the earthquake was 29.85 cm, yielding a maximum deflection of 33.54 m after accumulating deformation

during normal operations. For the ECFRD, the maximum deflection of the concrete-face slab increased to 31.21 cm, yielding a maximum deflection of 35.72 m after accumulating deformation during normal operations.

Figure 14 and Table 6 indicate that the maximum dynamic tensile stress along the slope of the CCFRD concrete-face slab caused by the earthquake was 2.84 MPa, which occurred on the left-hand side of the dam (at 2675 m elevation), while the maximum axial dynamic tensile stress was 2.47 Mpa. After the superposition of static and dynamic stresses, the tensile stress along the slope was 1.46 Mpa, which occurred at an elevation of 2695 m on the left-hand side of the dam, while the maximum axial tensile stress was 2.83 Mpa. For the ECFRD, the maximum dynamic tensile stress on the concrete-face slab along the slope was 3.55 Mpa, with a maximum axial dynamic tensile stress of 3.75 Mpa. After the superposition of static and dynamic stresses, the tensile stress along the slope was 1.34 Mpa and the maximum axial tensile stress was 2.66 Mpa. The areas in which these maxima occurred did not change significantly between the CCFRD and ECFRD cases.

**Table 6.** Maximum concrete-face slab deformation and strain in the CCFRD and ECFRD under earthquake action.

Deformation and Strain	CCFRD	ECFRD	Deformation and Strain	CCFRD	ECFRD
Deflection	29.85	31.21	Maximum axial dynamic tensile stress	2.47	3.75
Total deflection	33.54	35.72	Maximum dynamic tensile stress superposition in the slope direction	2.83	2.66
Maximum dynamic tensile stress in the slope direction	2.84	3.55	Maximum axial dynamic tensile stress superposition	1.46	1.34

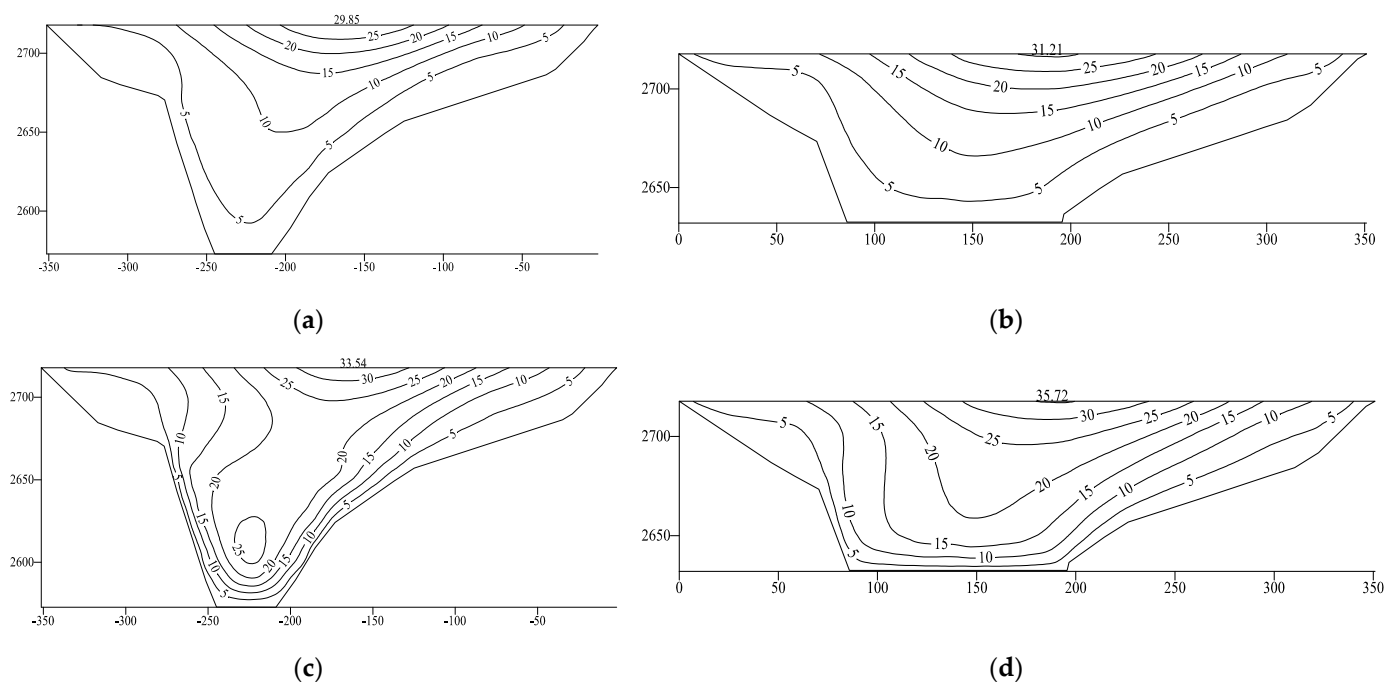


**Figure 13.** Calculated concrete-face slab deflection under earthquake conditions (cm). (a) Change in deflection for the CCFRD concrete-face slab; (b) Change in deflection for the ECFRD concrete-face slab; (c) Total change in deflection for the CCFRD concrete-face slab; (d) Total change in deflection for the ECFRD concrete-face slab.

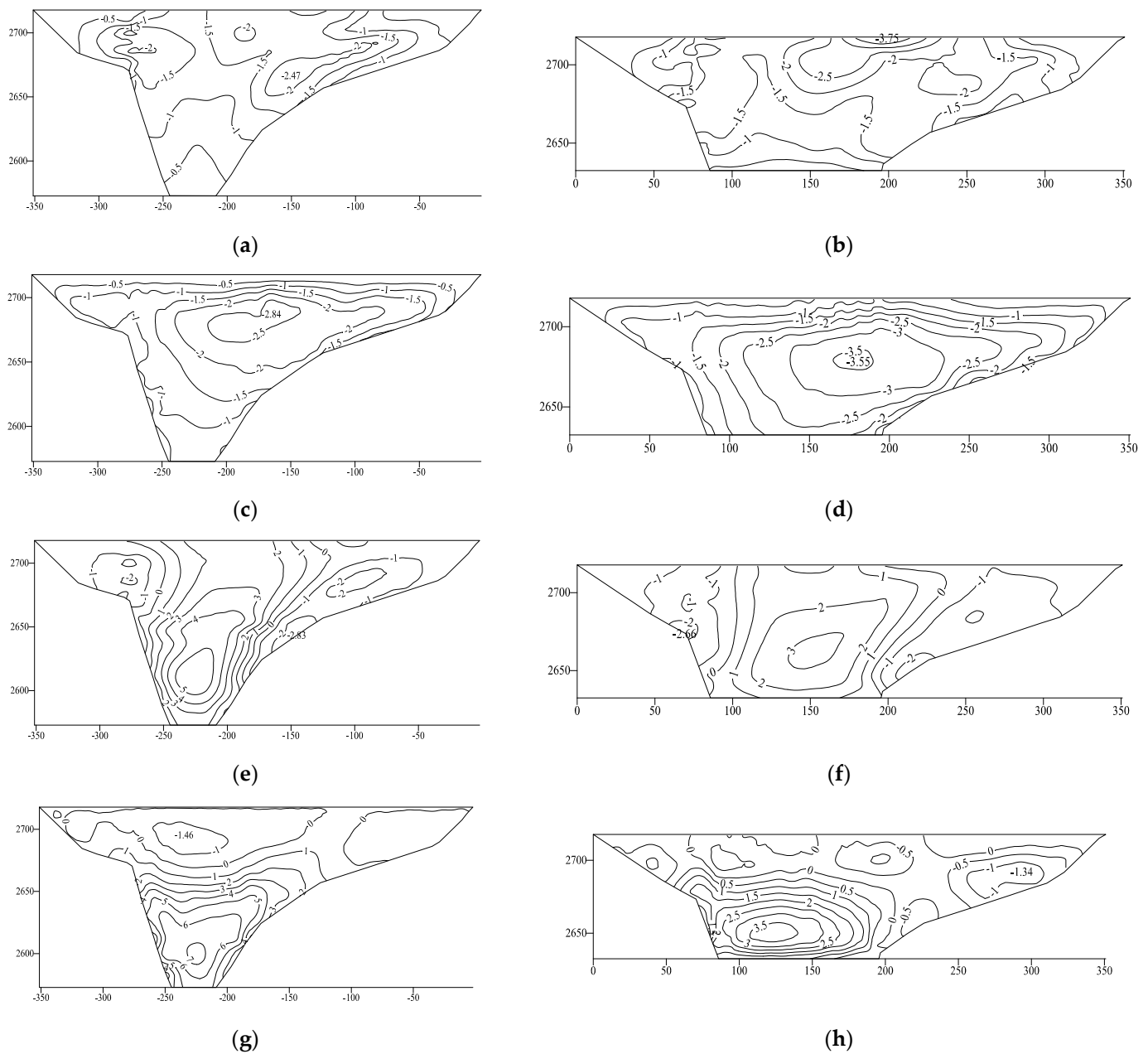


**Figure 14.** Stress results for the CCFRD and ECFRD concrete-face slab under earthquake conditions (MPa). (a) Maximum dynamic tensile stress on the CCFRD concrete-face slab along the slope; (b) Maximum dynamic tensile stress on the ECFRD concrete-face slab along the slope; (c) Maximum axial dynamic tensile stress on the CCFRD concrete-face slab; (d) Maximum axial dynamic tensile stress on the ECFRD concrete-face slab; (e) Maximum dynamic tensile stress superposition on the CCFRD concrete-face slab along the slope; (f) Maximum dynamic tensile stress superposition on the ECFRD concrete-face slab along the slope; (g) Maximum axial dynamic tensile stress superposition on the CCFRD concrete-face slab; (h) Maximum axial dynamic tensile stress superposition on the ECFRD concrete-face slab.

In contrast to the results obtained in the static analyses, the rockfill and concrete-face slab deformations were slightly higher in the ECFRD under earthquake conditions. The permanent seismic subsidence of the rockfill accounted for approximately 0.2% of the maximum dam height, which was within the empirical range of the permanent seismic deformation of a 150 m concrete-face rockfill dam. The maximum dynamic value of the CCFRD was approximately 1.7 times that of the maximum static value, while the max-

imum dynamic value of the ECFRD was approximately 2.9 times that of the maximum static value. In addition, the locations of the maximum static values differed. The location of the maximum static value was on the left-hand side of the dam at approximately 0.21–0.65 times the dam height. The influence of the permanent deformation of the rockfill dam on the maximum dynamic stress location occurred at the top of the left-hand  $0 + 174.5$  panel of the maximum cross-section of the rockfill dam. Simultaneously, the dynamic tensile stress on the concrete-face slab decreased owing to the effect of the embedded concrete body. Overall, the embedded concrete body improved the static stress–strain characteristics of the concrete-face rockfill dam at the hydropower station but was slightly unfavourable for its dynamic stress–strain state. However, the dynamic stress–strain parameters were within the allowable engineering range, and reinforcement methods could be used for the construction of ECFRD.

## 5. Conclusions

In this study, the ECFRD at a hydropower station in Qinghai Province, China was used as a case study site for three-dimensional finite element static and dynamic analyses. The influence of the embedded concrete body on the stress and strain characteristics of the rockfill and concrete-face slab was also analysed. The advantages of the embedded concrete body on the stability of the dam body were demonstrated, and the optimal height of the embedded concrete body was determined to provide a new design concept for the construction of 200–300 m concrete-face rockfill dams. The main conclusions can be summarised as follows:

1. Compared with a CCFRD, an embedded concrete body under a static load inhibited the static displacement of the rockfill along the river. When the height of the embedded concrete body was 40 m, the maximum horizontal displacements of the upstream and downstream rockfill were 2.1 and 0.6 cm less than those of the CCFRD, respectively. Moreover, owing to the stress on the embedded concrete body, the tensile stress along the slope of the concrete-face slab was completely eliminated, the axial stress was greatly reduced, the maximum deflection of the concrete-face slab decreased by 5.21 cm, and the area experiencing maximum stress shifted to 0.47 times the dam height.
2. Under the actions of dynamic and static–dynamic superposition, the deformation of the rockfill and concrete-face slab increased slightly, whereas the tensile stress on the concrete-face slab decreased slightly after setting the concrete-face slab. The permanent seismic subsidence of the rockfill body accounted for approximately 0.2% of the maximum dam height, the ratio of the maximum dynamic value to the maximum static value of the concrete-face slab increased from 1.7 to 2.9, and the cumulative static and dynamic value of the deflection of the concrete-face slab reached 35.72 m. Overall, the dynamic results for the ECFRD were within the controllable range of a 150 m concrete-face rockfill dam.
3. The ECFRD at the hydropower station was technically feasible and could effectively improve the static stress–strain characteristics of the dam body while shortening the length of the concrete-face slab and the joint. Under earthquake conditions, local reinforcement and other reinforcement measures could be applied to adapt the ECFRD to a 200–300 m high dam. For related projects, considering the project cost and stability of the embedded concrete body, we recommend that the height of the embedded concrete body should be 60 m, which is 0.4 times the height of the dam in this study.

**Author Contributions:** Conceptualisation, P.Q. and J.C.; methodology, P.Q. and J.C.; software, Z.X.; validation, Z.X.; formal analysis, P.Q.; investigation, P.Q.; resources, J.C.; data curation, P.Q.; writing—original draft, P.Q.; writing—review and editing, P.Q. and Z.X.; supervision, Z.X.; project administration, P.Q.; funding acquisition, J.C. and Z.X. All authors have read and agreed to the published version of the manuscript.

**Funding:** This study received financial support from the National Natural Science Foundation of China [grant number 52179143], Program 2022TD-01 for Shaanxi Provincial Innovative Research Team, and the Natural Science Foundation of Shanxi Province [grant number 2017JZ013].

**Data Availability Statement:** The original contributions presented in this study are included in this article. Further enquiries can be directed to the corresponding author.

**Acknowledgments:** We are very grateful to the anonymous reviewers for their constructive comments and suggestions.

**Conflicts of Interest:** The authors declare no conflict of interest.

## References

1. Li, J.; Lu, X.; Chen, J.; Yang, S.; Kuang, C.; Fan, Y.; Hu, K. Reliability-monitoring data coupled model for concrete slab safety evaluation of CFRD and its engineering application. *Structures* **2022**, *35*, 520–530. [\[CrossRef\]](#)
2. Khalid, M.I.; Park, D.; Fei, J.; Nguyen, V.; Nguyen, D.; Chen, X. Selection of efficient earthquake intensity measures for evaluating seismic fragility of concrete face rockfill dam. *Comput. Geotech.* **2023**, *163*, 105721. [\[CrossRef\]](#)
3. Xu, J.; Xu, H.; Yan, D.; Chen, K.; Zou, D. A Novel Calculation Method of Hydrodynamic Pressure Based on Polyhedron SBFEM and Its Application in Nonlinear Cross-Scale CFRD-Reservoir Systems. *Water* **2022**, *14*, 867. [\[CrossRef\]](#)
4. Dakoulas, P. Longitudinal vibrations of tall concrete faced rockfill dams in narrow canyons. *Soil Dyn. Earthq. Eng.* **2012**, *41*, 44–58. [\[CrossRef\]](#)
5. Zhao, W.; Wang, Z.; Zhang, H.; Wang, T. A Model Predicting the Maximum Face Slab Deflection of Concrete-Face Rockfill Dams: Combining Improved Support Vector Machine and Threshold Regression. *Water* **2023**, *15*, 3474. [\[CrossRef\]](#)
6. Shakarami, L.; Javdanian, H.; Zarif Sanayei, H.R.; Shams, G. Numerical investigation of seismically induced crest settlement of earth dams. *Model. Earth Syst. Environ.* **2019**, *5*, 1231–1238. [\[CrossRef\]](#)
7. Shao, L.; Wang, T.; Wang, Y.; Wang, Z.; Min, K. A Prediction Model and Factor Importance Analysis of Multiple Measuring Points for Concrete Face Rockfill Dam during the Operation Period. *Water* **2023**, *15*, 1081. [\[CrossRef\]](#)
8. Arici, Y. Evaluation of the performance of the face slab of a CFRD during earthquake excitation. *Soil Dyn. Earthq. Eng.* **2013**, *55*, 71–82. [\[CrossRef\]](#)
9. Nusier, O.K.; Alawneh, A.S. Kafrein Earth dam probabilistic seismic hazard assessment. *Soil Mech. Found. Eng.* **2006**, *43*, 211–215. [\[CrossRef\]](#)
10. Aman, S.; Rezk, M.A.; Nasr, R. Effect of Berm Properties on Non-Cohesive Earth Dam Failure due to Overtopping. *KSCE J. Civ. Eng.* **2023**, *27*, 1974–1984. [\[CrossRef\]](#)
11. Kim, Y.S.; Seo, M.W.; Lee, C.W.; Kang, G.C. Deformation characteristics during construction and after impoundment of the CFRD-type Daegok Dam, Korea. *Eng. Geol.* **2014**, *178*, 1–14. [\[CrossRef\]](#)
12. Liu, Y.; Zheng, D.; Cao, E.; Wu, X.; Chen, Z. Cracking risk analysis of face slabs in concrete face rockfill dams during the operation period. *Structures* **2022**, *40*, 621–632. [\[CrossRef\]](#)
13. Yao, F.H.; Guan, S.H.; Yang, H.; Chen, Y.; Qiu, H.F.; Ma, G.; Liu, Q.W. Long-term deformation analysis of Shuibuya concrete face rockfill dam based on response surface method and improved genetic algorithm. *Water Sci. Eng.* **2019**, *12*, 196–204. [\[CrossRef\]](#)
14. Xu, B.; Zou, D.; Kong, X.; Hu, Z.; Zhou, Y. Dynamic damage evaluation on the slabs of the concrete faced rockfill dam with the plastic-damage model. *Comput. Geotech.* **2015**, *65*, 258–265. [\[CrossRef\]](#)
15. Kartal, M.E.; Bayraktar, A.; Basaga, H.B. Nonlinear finite element reliability analysis of Concrete-Faced Rockfill (CFR) dams under static effects. *Appl. Math. Model.* **2012**, *36*, 5229–5248. [\[CrossRef\]](#)
16. Wen, L.; Chai, J.; Xu, Z.; Qin, Y.; Li, Y. Monitoring and numerical analysis of behaviour of Miaojiaba concrete-face rockfill dam built on river gravel foundation in China. *Comput. Geotech.* **2017**, *85*, 230–248. [\[CrossRef\]](#)
17. Mata, J.; Gomes, J.P.; Pereira, S.; Magalhaes, F.; Cunha, A. Analysis and interpretation of observed dynamic behaviour of a large concrete dam aided by soft computing and machine learning techniques. *Eng. Struct.* **2023**, *296*, 116940. [\[CrossRef\]](#)
18. Ghaemi, A.; Konrad, J.M. Empirical approaches to estimate the nonlinear dynamic responses of earth-core rockfill dams subjected to earthquake ground motions. *Soils Found.* **2022**, *62*, 101106. [\[CrossRef\]](#)
19. Wang, Y.; Wu, Z.; Qu, F.; Zhang, W. Numerical investigation on crack propagation process of concrete gravity dams under static and dynamic loads with in-crack reservoir pressure. *Theor. Appl. Fract. Mec.* **2022**, *62*, 101106. [\[CrossRef\]](#)

**Disclaimer/Publisher's Note:** The statements, opinions and data contained in all publications are solely those of the individual author(s) and contributor(s) and not of MDPI and/or the editor(s). MDPI and/or the editor(s) disclaim responsibility for any injury to people or property resulting from any ideas, methods, instructions or products referred to in the content.